Experimental frequency response evaluation for skyhook damping in an electrodynamic suspension testbench

Keyvan DELFARAH*, Marius PAKŠTYS*, Renato GALLUZZI**, Andrea TONOLI* and Nicola AMATI*
* Department of Mechanical and Aerospace Engineering, Politecnico di Torino
Turin, 10129, Italy
E-mail: marius.pakstys@polito.it
** School of Engineering and Sciences, Tecnologico de Monterrey
Mexico City, 14380, Mexico

Abstract
Magnetic levitation in the transportation field has been a subject of interest in recent decades. Its promising potential for high-speed applications makes it an appealing alternative to air travel and conventional rail for inter-urban connectivity. Several levitation architectures exist, being passive or active. The present work addresses the design, deployment, and experimental validation of a skyhook controller for improved passenger comfort in electrodynamically levitated transport systems. A dedicated test bench is outlined, and the system is represented by a multi-domain lumped parameter approach. Closed-loop skyhook control is included, and a discussion on system stability is made. A reduction in stability is noted for increasing skyhook damping, however no performance degradation is expected. Experimental validation in frequency domain is made, using capsule acceleration and chirp current signal data. Comparison with model output from MATLAB and Simulink shows an adequate conformity of the frequency responses for four cases of skyhook damping. Improvement of passenger comfort is also noted for lower frequencies. The study highlights a holistic evaluation of real electrodynamic levitation with skyhook control.

Keywords : Electrodynamic levitation, Skyhook control, Passenger comfort, Frequency domain, Maglev

1. Introduction

Magnetic levitation (maglev) systems offer a promising solution for ultra-high-speed transportation due to the absence of physical contact and friction. They represent an alternative solution to conventional rail and air travel in the scope of inter-urban connectivity, with purportedly lower power consumption. Maglev systems are distinguished by their control requirements into passive and active types. Electrodynamic suspension (EDS) systems as passive types require no active feedback and allow for larger air gaps, offering interesting potential. They are characterised by lift and drag force components, with drag reducing for increasing longitudinal speed. Several studies have been conducted to address their dynamic instability. One approach consists in adding a secondary suspension between the pad and capsule. In a simplified approach, the vertical dynamics of such system can be modelled resorting to a quarter car model (Galluzzi et al., 2020), commonly adopted in the automotive field, corresponding to a two degree-of-freedom (DOF) mechanical system. This system can be stabilised by properly selecting the secondary suspension stiffness and damping, as experimentally demonstrated by Tramacere et al. (2024). In addition to the instability issue, guaranteeing passenger comfort is another requirement of the secondary suspension (Nagai et al., 1989). In this regard, skyhook damping is a well-established method to enhance passenger comfort. It is implemented by producing a counteractive force through an actuator positioned between the sprung and unsprung masses (capsule and bogie, respectively). This has been explored by Negash et al. (2021) using a magnetorheological damper in hardware-in-the-loop tests for EDS systems. In the current study, the actuator is a voice coil positioned between the sprung and the unsprung masses that has been used to implement skyhook control. The aim of the current study is to design, implement, and experimentally validate a skyhook controller for a secondary suspension in an EDS system. Such analysis has so far been unexplored at a comprehensive level in literature. The validation is performed in frequency domain, with FRF computation between the voice coil actuator input and the sprung mass acceleration output.

The remainder of the manuscript is organised as follows. Section 2 gives an overview of the test equipment with key details. Section 3 provides a discussion on the modelling approach and the controller design. Section 4 outlines testing and comparison between experimental, numerical, and analytical results. Finally, Section 5 concludes the work.

2. Experimental setup

The test bench dedicated to studying the system is a dynamic testing setup comprised of sprung and unsprung masses representing the capsule and bogie, respectively, as per the quarter car approach. The sprung mass, m_s = 15.42 kg, and the unsprung mass, m_u = 4.2 kg. Secondary suspension stiffness k_s = 4422 N/m, and the stator stiffness k_u = 9700 N/m. A permanent magnet (PM) Halbach array is coupled to the unsprung mass, consisting of N45UH NdFeB magnets. A rotating copper rim facilitates the equivalent relative longitudinal speed v between track and PM array necessary to levitate the masses. It is driven by a Kollmorgen AKD/AKM servomotor. A MEMS accelerometer (MPU 9250) is mounted on each mass. Only the sprung mass accelerometer is used for feedback control. A voice coil actuator (Geeplus VM108-2P30) is assembled between the two masses such that control actions are facilitated. It can exert a maximum force of 230 N. The force-current factor, K_m = 25 N/A and the back-EMF constant, K_v = 25 Vs/m. The subsystem also features a winding resistance of 1.43 Ω and an inductance of 11.1 mH. Its inherent damping is c_s = 207 Ns/m. The equipment is equivalent to that used by Tramacere et al. (2024). Figure 1(a) indicates the experimental test equipment.

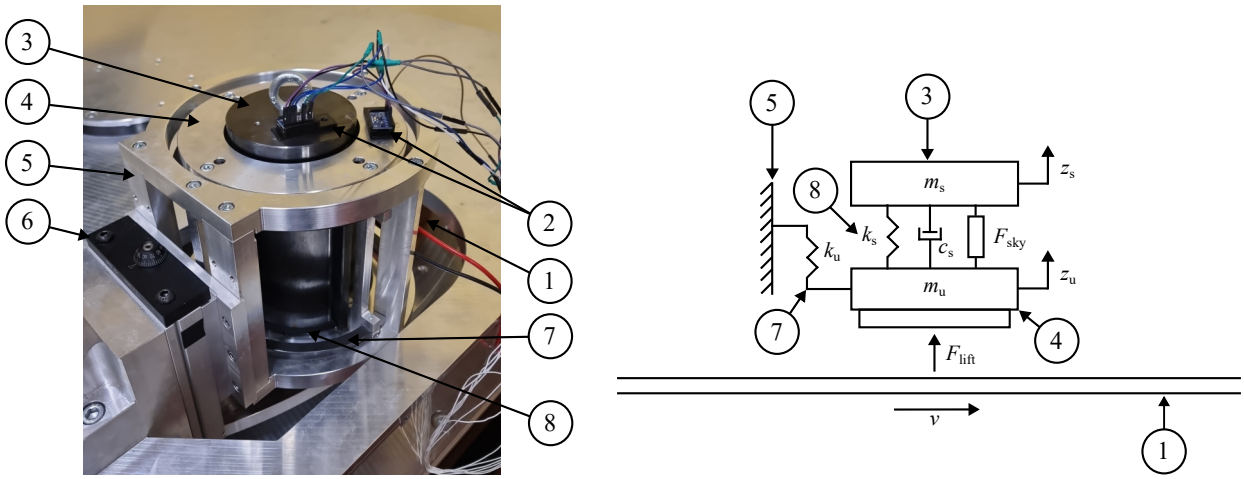

Fig. 1 Mechanical and electrodynamic system. (a) Dynamic testing stage. 1. Copper track; 2. MPU 9250 accelerometers; 3. Sprung mass; 4. Unsprung mass; 5. Stator; 6. Micro-metric stage; 7. Unsprung mass–stator flex hinge; 8. Sprung–unsprung mass flex hinge. (b) Two-DOF quarter car model representing the electrodynamic levitation dynamic testing stage.

Control actions are computed on a TI F28379D LaunchPad control card, exploiting generated code from MATLAB and Simulink. A TI BOOSTXL DRV8323RS power stage is coupled to the microprocessor, receiving pulse-width modulation commands and coupled to a power supply. The experimental setup outputs sprung mass acceleration and voice coil current. The setup receives voice coil voltage and track irregularities as control input (including current perturbation) and external disturbance, respectively.

3. Modelling

The system is modelled with a multi-domain lumped parameter approach (Galluzzi et al., 2020) for numerical and analytical analysis in MATLAB and Simulink. The electrodynamic levitation phenomenon is represented by an equivalent electrical circuit featuring a voltage source and parallel branches each containing a resistance and inductance in series. Increasing the number of branches reduces the fit error. Equations (1) and (2) represent the coupled electrical circuit direct

current $i_{\mathrm{d},k}$, and quadrature current $i_{\mathrm{q},k}$ components for the kth branch.

$$\frac{\mathrm{d}i_{\mathrm{d},k}}{\mathrm{d}t} = -\omega_{\mathrm{p},k} i_{\mathrm{d},k} + \omega i_{\mathrm{q},k} - \frac{\partial \Lambda}{\partial z_{\mathrm{p}}} \frac{\dot{z}_{\mathrm{u}}}{L_k} \tag{1}$$

$$\frac{\mathrm{d}i_{\mathrm{q},k}}{\mathrm{d}t} = -\omega_{\mathrm{p},k} i_{\mathrm{q},k} - \omega i_{\mathrm{d},k} - \frac{\Lambda \omega}{L_k} \tag{2}$$

Note that $\omega_{\mathrm{p},k}$ and L_k denote the electrodynamic pole frequency and inductance of the kth branch. The term ω refers to the excitation frequency as a function of longitudinal speed. Flux linkage and unsprung mass displacement are indicated with Λ and z_{u} respectively.

The model is fitted to experimental data, and linearised around a nominal air gap, $z_{\mathrm{u},0}$, reported in Eq. (3), with Eq. (4) defining the frequency-dependent term, Γ, implicitly considering longitudinal speed.

$$z_{\mathrm{u},0}(\omega) = -\frac{\gamma}{2} \ln\left(\frac{(m_{\mathrm{s}} + m_{\mathrm{u}}) \mathrm{g} \gamma}{\Lambda_0^2 \Gamma(\omega)} \right) \tag{3}$$

$$\Gamma(\omega) = \sum_{k=1}^{N_{\mathrm{b}}} \left(\frac{\omega^2 / \omega_{\mathrm{p},k}^2}{L_k \left(1 + \omega^2 / \omega_{\mathrm{p},k}^2 \right)} \right) \tag{4}$$

The magnetic pole pair pitch ratio is referred to as γ. The unsprung and sprung masses are denoted as m_{u} and m_{s} respectively. The unsprung mass refers to the bogie and the sprung mass to the capsule. Flux linkage amplitude is Λ_0 and acceleration due to gravity is g. The term N_{b} indicates the number of parallel branches in the circuit.

The EDS system is modelled with two parallel branches. The branch electrodynamic pole frequencies are $\omega_{\mathrm{p},1} = 233.2$ rad/s and $\omega_{\mathrm{p},2} = 1.43 \times 10^3$ rad/s. Branch inductances are $L_1 = 108.4$ mH and $L_2 = 179.9$ mH, corresponding to a selection of flux linkage amplitude $\Lambda_0 = 1$ Wb. Branch resistances can be computed with $\omega_{\mathrm{p},k} = R_k / L_k$.

The mechanical domain is modelled with the quarter car approach, featuring a secondary suspension and the aforementioned masses. The contribution of the voice coil in electrical domain is also included. Equations (5) to (7) represent the system considering electrodynamic and voice coil force contributions.

$$\ddot{z}_{\mathrm{u}} = -\frac{c_{\mathrm{s}}}{m_{\mathrm{u}}} \dot{z}_{\mathrm{u}} + \frac{c_{\mathrm{s}}}{m_{\mathrm{u}}} \dot{z}_{\mathrm{s}} - \frac{k_{\mathrm{s}} + k_{\mathrm{u}}}{m_{\mathrm{u}}} z_{\mathrm{u}} + \frac{k_{\mathrm{s}}}{m_{\mathrm{u}}} z_{\mathrm{s}} - \frac{K_{\mathrm{m}}}{m_{\mathrm{u}}} i_{\mathrm{vc}} + \frac{F_{\mathrm{u}}}{m_{\mathrm{u}}} - \frac{2\Lambda_0}{\gamma m_{\mathrm{u}}} e^{\frac{z_{\mathrm{u},0}}{\gamma}} \sum_{k=1}^{N_{\mathrm{b}}} i_{\mathrm{d},k} \tag{5}$$

$$\ddot{z}_{\mathrm{s}} = \frac{c_{\mathrm{s}}}{m_{\mathrm{s}}} \dot{z}_{\mathrm{u}} - \frac{c_{\mathrm{s}}}{m_{\mathrm{s}}} \dot{z}_{\mathrm{s}} + \frac{k_{\mathrm{s}}}{m_{\mathrm{s}}} z_{\mathrm{u}} - \frac{k_{\mathrm{s}}}{m_{\mathrm{s}}} z_{\mathrm{s}} + \frac{K_{\mathrm{m}}}{m_{\mathrm{s}}} i_{\mathrm{vc}} + \frac{F_{\mathrm{s}}}{m_{\mathrm{s}}} \tag{6}$$

$$\frac{\mathrm{d}i_{\mathrm{vc}}}{\mathrm{d}t} = \frac{K_{\mathrm{v}}}{L_{\mathrm{vc}}} \dot{z}_{\mathrm{u}} - \frac{K_{\mathrm{v}}}{L_{\mathrm{vc}}} \dot{z}_{\mathrm{s}} - \frac{R_{\mathrm{vc}}}{L_{\mathrm{vc}}} i_{\mathrm{vc}} + \frac{V}{L_{\mathrm{vc}}} \tag{7}$$

The secondary suspension (sprung–unsprung mass) stiffness and damping are k_{s} and c_{s} respectively. Stiffness between unsprung mass and stator is k_{u}. Sprung mass displacement is given by the term z_{s}. The force-current factor of the voice coil is K_{m} while its back-EMF constant is K_{v}. Voice coil current is indicated with i_{vc} and voltage across its terminals with V. External forces incident on the unsprung and sprung masses are F_{u} and F_{s} respectively.

Electrical and mechanical domains are assembled in state space representation. The model is characterised by two inputs and three outputs. Track irregularities z_t and voice coil voltage are inputs. Voice coil current and sprung mass acceleration are outputs. The model reflects experimental inputs and outputs.

The total force in a secondary suspension including a real skyhook damping contribution, $F_{\mathrm{t,sky}}$, is given by Eq. (8). The skyhook damping value is given by c_{sky}.

$$F_{\mathrm{t,sky}} = -c_{\mathrm{sky}} \dot{z}_{\mathrm{s}} - c_{\mathrm{s}} (\dot{z}_{\mathrm{s}} - \dot{z}_{\mathrm{u}}) \tag{8}$$

Closed-loop control is implemented by exploiting the computed sprung mass velocity. Figure 2(a) indicates the control scheme. Sprung mass acceleration is integrated and a high-pass filter with cut-off frequency of 5 Hz, G_{HPF}, is applied to ensure drift mitigation. The skyhook damping gain is applied and a reference current, i_{con}, is obtained using the voice coil force constant K_{m}. Skyhook damping and voice coil force constant are combined in a condensed gain, G_{sky}. The current error, i_{err}, is obtained considering the measured coil current, i_{coil}, the offset current, i_{off}, and the chirp signal current, i_{chirp}. The chirp signal represents an FRF input of the study. Frequency sweep varies linearly from 1 Hz to 100 Hz in 100 s. Current amplitude is set to 0.5 A. A Proportional-Integral (PI) controller, G_{PI}, guarantees the voltage setpoint, V.

PI bandwidth is limited to 150 Hz. Current controller gains are selected based on the voice coil electrical characteristics and desired bandwidth. Track irregularities are numerically modelled by exploiting profile measurements by Tramacere et al. (2024), using a sinusoidal approximation approach. The control scheme (including current perturbation) is deployed experimentally and replicated numerically.

System stability under varying skyhook damping gain is analytically evaluated. The real part of the most critical pole is computed for each skyhook damping parameter selection. Figure 2(b) indicates the stability tendency. It is evident that a skyhook damping of 300 Ns/m guarantees optimal stability, however a further improved passenger comfort condition is attained at higher skyhook damping values. Despite deteriorating stability, the system is expected to perform robustly enough at higher skyhook damping values. Indeed, stability worsens marginally beyond 1500 Ns/m.

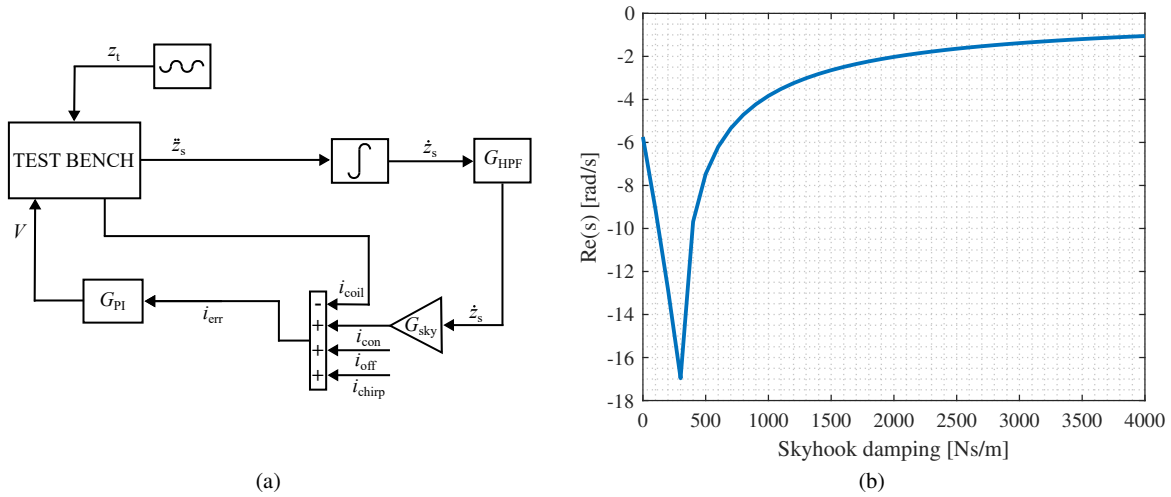

(a) (b)

Fig. 2 (a) Control scheme for numerical and experimental implementation. Track irregularities z_t are incident on the system. A high-pass filter, G_{HPF} ensures drift mitigation. A reference current, i_{con}, is generated from the condensed skyhook gain G_{sky}. The current error, i_{err}, considers measured coil current, i_{coil}, the offset current, i_{off}, and the chirp signal current, i_{chirp}. The Proportional-Integral (PI) controller, G_{PI}, guarantees the voltage setpoint, V. (b) Stability analysis for skyhook damping. Optimal stability corresponds to 300 Ns/m. Increased passenger comfort is attained at higher skyhook damping values, with acceptable stability reduction.

4. Testing and results

MATLAB and Simulink are used to communicate with the TI F28379D LaunchPad via serial bus. The user can modify several parameters on-line using a dedicated host model. A voltage offset is given to separate the sprung and unsprung masses. The desired skyhook damping is updated on-line by the user. A speed setpoint of 500 rpm is given to the servomotor, initiating track rotation. When steady-state conditions are reached, the chirp signal is enabled, and acceleration is sampled together with the imposed current perturbation. Several skyhook damping gains are evaluated. A baseline test is made with a skyhook gain of 0 Ns/m. Then, closed-loop tests are made imposing skyhook damping values of 500 Ns/m, 1000 Ns/m, and 2000 Ns/m. Sampled data are post-processed to compute the FRF.

Additionally to experimental evaluation, a Simulink model of the system is used for FRF comparison. The FRF is also calculated analytically. The modelling approach is that described in Section 3.

Figure 3(a) reports the FRF for the baseline system. Both analytical and numerical models adequately conform to the experimental data. Note that harmonic contributions stemming from track irregularities are evident in the computed FRF for both experimental and numerical cases. Similarly, Fig. 3(b), Fig. 4(a), and Fig. 4(b) show the system responses for skyhook damping of 500 Ns/m, 1000 Ns/m, and 2000 Ns/m, respectively. A slight distortion is noted for low frequencies due to filtering effects. The correspondence between analytical, numerical, and experimental FRFs is likewise noted to be adequate.

Moreover, a reduction in output sprung mass acceleration magnitude with respect to input voice coil current perturbation is evident for lower frequency ranges. Since the sprung mass natural frequency is lower than that of the unsprung mass, this reflects the aim of skyhook damping. Passenger comfort can be improved with the implementation of skyhook damping in a secondary suspension system of a maglev vehicle. Experimental validation of the model further allows for

the analysis of varying control parameters before deployment.

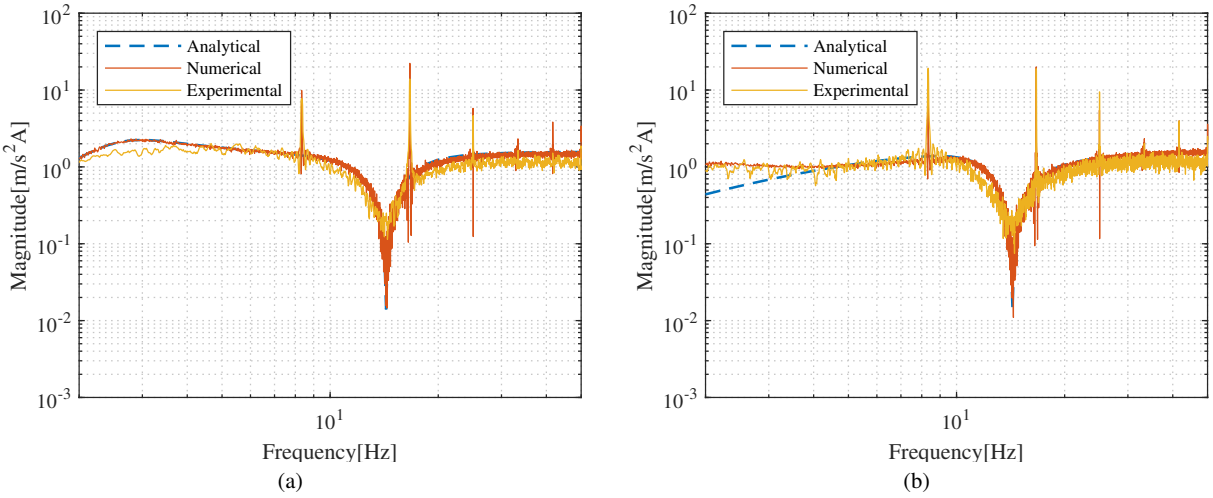

Fig. 3 Frequency response functions for output sprung mass acceleration and input current perturbation at a track speed of 500 rpm. (a) Analytical, numerical, and experimental FRFs for $c_{\mathrm{sky}} = 0$ Ns/m. (b) Analytical, numerical, and experimental FRFs for $c_{\mathrm{sky}} = 500$ Ns/m.

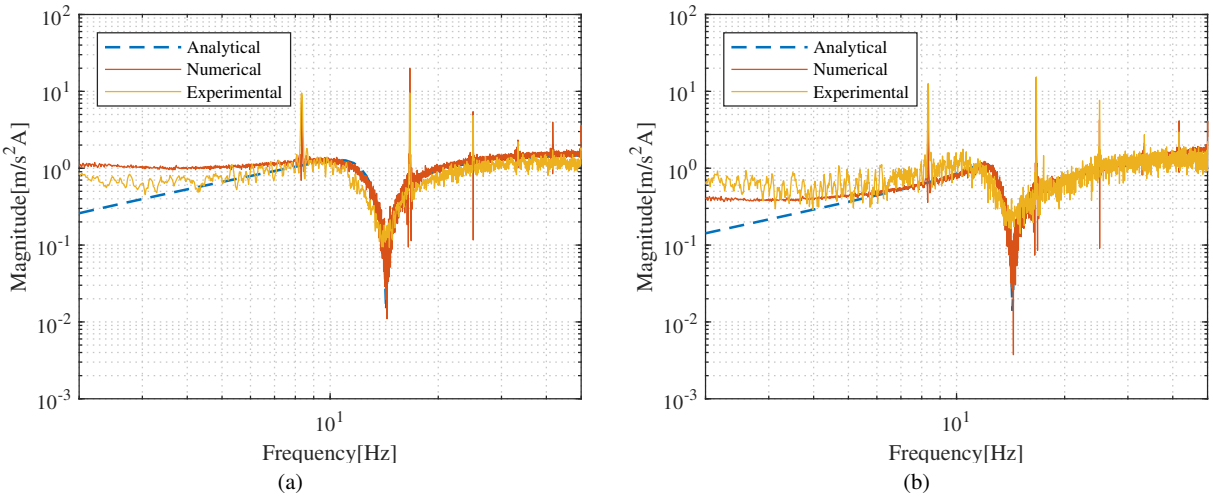

Fig. 4 Frequency response functions for output sprung mass acceleration and input current perturbation at a track speed of 500 rpm. (a) Analytical, numerical, and experimental FRFs for $c_{\mathrm{sky}} = 1000$ Ns/m. (b) Analytical, numerical, and experimental FRFs for $c_{\mathrm{sky}} = 2000$ Ns/m.

5. Conclusions

In this work, a comparison and validation in frequency domain between numerical modelling and experimental testing is performed for an electrodynamic levitation system with skyhook damping. Closed-loop control is shown, and passenger comfort is targeted. An overview of a dedicated test bench is presented. The EDS phenomenon is modelled using a two-branch equivalent electrical circuit. A two-DOF quarter car model represents the system in mechanical domain. Skyhook damping is implemented considering a control action exerted by a voice coil actuator. It is represented as a viscous damper depending only on sprung mass velocity. The voice coil actuator is represented by its electrical expression. The model is exploited both analytically and numerically in Simulink for FRF comparison. A low skyhook damping value corresponds to the optimal stability case, however improving passenger comfort demands larger gains, paired with a worsening stability condition. Stability is nonetheless conserved for increased skyhook damping values. On the experimental side, sampled sprung mass acceleration and current perturbation are used to determine the frequency response. Results display a notably good conformity between the analytical and numerical models with respect to the

experimental data, in a comparison for four skyhook damping gains. Moreover, an improvement in passenger comfort is noted in the response for lower frequencies. The feasibility of using active control in the secondary suspension of an EDS system is comprehensively demonstrated.

Future work involves the analysis of changing mechanical parameters, such as mass. System response at different speeds is also of interest. The evaluation of skyhook and groundhook combination is additionally important to understand the effects on the unsprung mass, and to mitigate variation in longitudinal drag.

References

R. Galluzzi, S. Circosta, N. Amati, A. Tonoli, A. Bonfitto, T. A. Lembke, M. Kertész (2020). A Multi-domain Approach to the Stabilization of Electrodynamic Levitation Systems. Journal of Vibration and Acoustics, 12.

M. Nagai, A. Moran, S. Tanaka (1989). Optimal Active Suspension to Improve the Dynamic Stability of Repulsive MAGLEV Systems.

B. A. Negash, W. You, J. Lee, C. Lee, K. Lee (2021). Semi-Active Control of a Nonlinear Quarter-Car Model of Hyperloop Capsule Vehicle with Skyhook and Mixed Skyhook-Acceleration Driven Damper Controller. Advances in Mechanical Engineering, vol. 13, no. 2, Feb. 2021, p. 168781402199952. DOI.org (Crossref), https://doi.org/10.1177/1687814021999528.

E. Tramacere, M. Pakštys, R. Galluzzi, N. Amati, A. Tonoli, T. A. Lembke (2024). Modeling and Experimental Validation of Electrodynamic Maglev Systems. Journal of Sound and Vibration, vol. 568, Jan. 2024, p. 117950. DOI.org (Crossref), https://doi.org/10.1016/j.jsv.2023.117950.